

Published in final edited form as:

Angew Chem Int Ed Engl. 2011 June 27; 50(27): 6109–6114. doi:10.1002/anie.201100884.

Tunable, Ultra-Sensitive pH Responsive Nanoparticles Targeting Specific Endocytic Organelles in Living Cells**

Kejin Zhou⁺,

Department of Pharmacology, Simmons Comprehensive Cancer Center, UT Southwestern Medical Center at Dallas, 5323 Harry Hines Blvd, Dallas, Texas 75390 (USA), Fax: (+ 1) 214-648-7084, jinming.gao@utsouthwestern.edu

Yiguang Wang⁺,

Department of Pharmacology, Simmons Comprehensive Cancer Center, UT Southwestern Medical Center at Dallas, 5323 Harry Hines Blvd, Dallas, Texas 75390 (USA), Fax: (+ 1) 214-648-7084, jinming.gao@utsouthwestern.edu

Xiaonan Huang⁺,

Department of Pharmacology, Simmons Comprehensive Cancer Center, UT Southwestern Medical Center at Dallas, 5323 Harry Hines Blvd, Dallas, Texas 75390 (USA), Fax: (+ 1) 214-648-7084, jinming.gao@utsouthwestern.edu

Katherine K. Luby-Phelps,

Department of Cell Biology, UT Southwestern Medical Center at Dallas, Dallas, Texas 75390 (USA)

Baran D. Sumer, and

Department of Otolaryngology, UT Southwestern Medical Center at Dallas, Dallas, Texas 75390 (USA)

Jinming Gao

Department of Pharmacology, Simmons Comprehensive Cancer Center, UT Southwestern Medical Center at Dallas, 5323 Harry Hines Blvd, Dallas, Texas 75390 (USA), Fax: (+ 1) 214-648-7084, jinming.gao@utsouthwestern.edu

In recent years, multifunctional nanoparticles have received considerable attention in many applications such as biosensors, diagnostic nanoprobe and targeted drug delivery.^[1] These efforts have been driven to a large extent by the need to improve biological specificity in diagnosis and therapy through the precise, spatio-temporal control of agent delivery. In order to achieve this goal, continuous efforts have been dedicated to develop stimuli-responsive nanoplatfroms.^[2] Environmental stimuli that were exploited include pH,^[3] temperature,^[4] enzymatic expression,^[5] redox reaction^[6] and light induction.^[7] Among these activating signals, pH trigger is one of the most extensively studied stimuli based on two types of pH differences: (a) pathological (e.g. tumor) vs. normal tissues and (b) acidic intracellular compartments.^[8] For example, due to the unusual acidity of the tumor extracellular microenvironment ($\text{pH}_e \approx 6.5$), several pH_e -responsive nanosystems were reported to increase the sensitivity of tumor imaging or the efficacy of therapy.^[9]

**This work was supported by the NIH (R01CA129011 and R21EB005394). We thank Prof. R.G.W. Anderson for helpful discussions on cell internalization studies, E. Ross and M. Evans for stopped flow experiments and M. Poudel for fluorescence life time measurements.

⁺These authors contributed equally to this work.

Supporting information for this article is available on the WWW under <http://www.angewandte.org> or from the author.

To target the acidic endo-/lysosomal compartments, nanovectors with pH-cleavable linkers were reported to improve payload bioavailability.^[10] Furthermore, several smart nanovectors with pH-induced charge conversion were designed to increase drug efficacy.^[11] Despite these remarkable advances, specific transport and activation of nanoparticles in different endocytic organelles during endocytosis in living cells is not well documented.^[12] The endocytic system is comprised of a series of compartments that have distinctive roles in the sorting, processing and degradation of internalized cargo. Selective targeting of different endocytic compartments by pH-sensitive nanoparticles is challenging due to the short nanoparticle residence times (~mins) and small pH differences in these compartments (e.g. <1 pH unit between early endosomes and lysosomes).^[13]

Herein we report a set of tunable, pH-activatable micellar (pHAM) nanoparticles based on the supramolecular self-assembly of ionizable block copolymer micelles (Figure 1). Micelle formation and its thermodynamic stability are driven by the delicate balance between the hydrophobic and hydrophilic segments.^[14] Ionizable groups can act as tunable hydrophobic groups at different pH values. Amino groups have been incorporated into polymers as ionizable groups to render pH sensitivity.^[15] In this study, we introduced tertiary amines with precisely controlled hydrophobic substituents as ionizable hydrophobic blocks. Micellization dramatically sharpens the ionization transition of tertiary amines in the hydrophobic block, rendering fast and ultra-sensitive pH response. Nanoparticles with different transition pH can be selectively activated in specific endocytic compartments such as early endosomes or lysosomes in human cells.

For proof of concept, we synthesized two series of block copolymers (PEO-*b*-PR, Figure 1) with tertiary amine-containing (PR) and poly(ethylene oxide) (PEO) segments by atom transfer radical polymerization (Supplementary Table S1).^[16] In the linear di-alkyl series, we varied the chain length from methyl to butyl groups; in the cyclic series, we varied the ring size from 5- to 7-membered rings. The two series were systematically used to adjust the pKa values of ammonium groups (Supplementary Table S2) and PR hydrophobicity. A pH-insensitive dye, tetramethyl rhodamine (TMR),^[17] was used as a model fluorophore and conjugated in the PR block as an imaging beacon to investigate the pH responsive properties. At higher pH, neutral PR segments self-assemble into the hydrophobic cores of micelles, resulting in the aggregation of fluorophores and quenching of fluorescent signals through mechanisms of Förster resonance energy transfer between TMR molecules (homo-FRET) and photoinduced electron transfer (PeT) from tertiary amines to TMR.^[18] At lower pH, PR segments become protonated and positively charged, leading to micelle disassembly and dramatic increase in fluorescence emission due to the increase in TMR distance and decrease in PeT (Figure 1).

Fluorescent images of a series of nanoprobe solutions (Figure 2a) at different pH values illustrate a sharp fluorescence transition for each nanoprobe. In this study, poly(ethylene oxide)-*b*-poly((dimethyl-amino)ethyl methacrylate) (PEO-*b*-PDMA, **1**) was used as an “always ON” control where no micelles or fluorescence quenching was observed in the tested pH range (4.5–8.0) due to the strong hydrophilicity of the PDMA block (see discussion below). Normalized fluorescence intensity (NFI) vs. pH curves (Figure 2b) allowed for quantitative assessment of the ultra-pH responsive properties. NFI is calculated as the ratio of $[F - F_{\min}] / [F_{\max} - F_{\min}]$, where F is the fluorescence intensity of the nanoprobe at any given pH, and F_{\max} and F_{\min} are the maximal and minimal fluorescence intensities at the ON/OFF states, respectively. To quantify the sharpness in pH response, we evaluated $\Delta\text{pH}_{10-90\%}$, the pH range in which the NFI value varies from 10% to 90%, for all the pHAM nanoprobos. The sharpness values were 0.21, 0.23, 0.24, and 0.20 pH unit for nanoprobos **4**, **6**, **3** and **7**, respectively. The small values indicate a remarkable pH sensitivity as it represents a <2-fold change in proton concentration. In comparison, for small molecular

dyes^[19], the sharpness value is about 2 pH unit (100-fold in $[H^+]$) for the same degree of emission change, consistent with Henderson-Hasselbalch equation^[20]. In addition to the pH sharpness, we also measured the ratio of F_{max} and F_{min} ($R_F = F_{max}/F_{min}$) to quantify the fluorescence response between the ON/OFF states. The values of R_F range from 10 to 55 fold (Table S2, Figure S1). Consistent with the decreased emission intensity in the micelles, data show that excited state of TMR had a much shorter life time (e.g. 0.44 ns for nanoprobe **3**, Figure S2) in the micelles (pH = 7.4) than the free dye (1.97 ns) at pH 7.4 or the disassembled unimers at pH 5.5 (1.84 ns).

For the pH temporal reponse, stopped-flow experiments showed that fluorescence activation was very fast, with most nanoprobe fully activated within 5 ms at lower pH (e.g. $\tau_{1/2} = 3.7$ ms for **4**, Figure 2c). The ultra-sensitive pH response was only observed with **4**, **3**, **7** and **6**. The fluorescence transition pH values (pH_t , the pH at which $F = 0.5 \times (F_{max} + F_{min})$) were 5.4, 6.3, 6.8 and 7.2 for nanoprobe **4**, **3**, **7** and **6**, respectively (Figure 2b). The other copolymers either did not show any pH response (e.g., **1** in Figure 2a) or only broad pH responses (e.g. **2**, **5**, data not shown). We hypothesize that hydrophobic micellization is the driving force of the ultra-pH responsive properties of pHAM, and a critical threshold of hydrophobicity in the PR segment is necessary to achieve the co-operative response. To test this hypothesis, we used copolymers **5** and **7** as examples and compared their pH titration curves as well as the corresponding monomers (Figure 3a). Larger ring size (i.e. **7**) resulted in higher hydrophobicity in the PR segment due to the extra methylene groups. Copolymer **5** showed a broad pH response, similar to both monomers over added volumes of NaOH. In contrast, copolymer **7** had a dramatically sharpened pH transition, demonstrating a greatly increased buffer capacity. Deuterated 1H NMR spectra of **5** and **7** at different ionization states of tertiary amines further support the hypothesis (Figure 3b). The PEO segment did not change its peak intensity and was used as an internal standard. Throughout the ionization states, the proton resonance peaks for the PR segment of **5** were easily visualized although the peak intensity decreased with broadened peak width at higher pH, reflecting the bulk aggregation behavior of the copolymer. For **7**, neutral state of the copolymer (i.e. 0%) led to completely suppressed resonance peaks in the PR segment due to the formation of highly compact micelle cores. Transmission electron microscopy (TEM) of **7** in aqueous solution demonstrated the formation of micelles above its pK_a (6.7) at pH 7.4 and complete micelle dissociation at pH 5.5 (Figure 3c). In comparison, no micelles were formed from **5** at either pH (data not shown).

To investigate the intracellular activations of pHAM, we examined nanoprobe **3** in human H2009 lung cancer cells by confocal laser scanning microscopy (Figure S3). It should be noted that nanoprobe **3** has an optimal pH transition at 6.3, which is ideally suited for the study of nanoparticle activation in early endosomes (pH = 5.9–6.2)^[13a, 21]. Because pHAM nanoprobe are “silent” at neutral pH, we directly applied them in the culture medium and monitored the kinetics of their uptake and activation without the need to remove the medium. Right after the nanoprobe addition, neither the H2009 cells nor the medium showed observable fluorescence signal. At 15 min, punctuate fluorescent dots appeared inside the cells. The number of fluorescent dots increased over time. Signal to noise ratio of the H2009 cells (SNR_{Cell} , using fluorescence intensity at time 0 as the background noise) allowed further quantification of the increased nanoprobe uptake and activation over time. At 60 min, a 31-fold increase in SNR_{Cell} ($2.14 \pm 0.17 \times 10^3$) was observed over the medium ($SNR_{Med} = 69.3 \pm 9.1$, $P < 0.001$) where majority of the nanoprobe were still present. Then 0.1N HCl solution was added to acidify the medium pH to 5.0 and considerable increase in fluorescence intensity in the medium background was found. A reverse trend of fluorescence contrast was observed, where SNR_{Cell} was 74% of SNR_{Med} ($P < 0.05$). These data illustrate that pHAM nanoprobe can dramatically increase the contrast sensitivity of cancer cells compared to potentially always ON nanoprobe (as in the case after HCl was added).

To further investigate whether different endocytic organelles can selectively activate pHAM, we transfected H2009 cells with green fluorescent protein (GFP)-fused Rab5a and Lamp1 biomarkers in early endosomes and late endosomes/lysosomes, respectively. Two pHAM nanoprobe (3 and 4 with pH_t of 6.3 and 5.4, respectively) were incubated with H2009 cells and confocal imaging was used to examine the subcellular locations for pHAM activation (Figure 4 and Figure S4). H2009 cells ($N=30-50$) with 20 or more colocalized dots (i.e. activated pHAM within early endosomes or lysosomes) were identified as positive and the percentage was quantified (Figure 4c and 4d). For nanoprobe 3, 80% of cells were positive in colocalization with early endosomes at 30 min, whereas only 12% colocalized with late endosomes/lysosomes (Figure 4a and Figure S4). Over time, colocalization of activated 3 decreased with early endosomes but increased with late endosomes/lysosomes (Figure 4c). In contrast, nanoprobe 4 ($pH_t = 5.4$) showed a different pattern of subcellular location for activation. At all times, less than 10% of positive cells were found with early endosome colocalization (top panel of Figure 4b and Figure S4). Instead, almost all the activated nanoprobe 4 colocalized with late endosomes/lysosomes (Figure 4b bottom panel, Figure 4d). Figure 4e and Figure 4f depict the different processes of intracellular uptake and activation of the two nanoprobe. Nanoprobe 3 can be quickly activated inside early endosomes with higher vesicular pH (5.9–6.2)^[13a, 21] and the activation is sustained as the nanoprobe traffic into late endosomes/lysosomes. By contrast, nanoprobe 4 is almost exclusively activated inside the late endosomes/lysosomes with lower vesicular pH (5.0–5.5).^[13a, 21] Similar results were also found with human SLK tumor endothelial cells (data not shown). These data demonstrate the feasibility of targeting small differences in the vesicular pH inside different endocytic organelles by the pHAM nanoparticles.

To verify the intracellular activation mechanism of pHAM, we incubated H2009 cells with bafilomycin A1 for 1 hour and then added nanoprobe 3. Bafilomycin is a specific inhibitor of vacuolar-type H^+ -ATPase (V-ATPase),^[22] which is responsible for the proton pumping across the plasma membranes and acidification of intracellular organelles (e.g. lysosomes). Data show that in the presence of bafilomycin A1, nanoprobe 3 was not activated as indicated by the absence of TMR fluorescence (Figure 5a). After removal of bafilomycin A1 and 3 in the culture medium, the activation of 3 emerged with colocalization of TMR fluorescence with GFP labeled lysosomes (Figure 5b). Similar results were also found with nanoprobe 4 in H2009 cells (Figure S5).

In summary, we report the design of a series of pH-activatable micellar nanoparticles with tunable and ultra-sensitive pH response in the physiological range (5.0–7.4). These nanopartilces have fast temporal response (<5 ms), large increase of emission intensity between ON/OFF states (up to 55 times), and only require <0.25 pH for activation. Confocal imaging studies demonstrate the nanoparticles are “silent” in the media at pH 7.4 but can be activated upon uptake in cells. Moreover, nanoparticles with pH transitions at 6.3 and 5.4 can be selectively activated in different endocytic compartments such as early endosomes (pH 5.9–6.2) and lysosomes (5.0–5.5). This nanoplatform offers many exciting opportunities in the development of nonlinear ON/OFF nanosystems for diagnostic imaging and drug delivery applications with minimal effect at physiological pH (e.g. 7.4), but can be activated in acidic tumor pH or specific intracellular organelles (e.g. endosomes/lysosomes) upon uptake in targeted cells.

Supplementary Material

Refer to Web version on PubMed Central for supplementary material.

References

1. a) Singhal S, Nie S, Wang MD. *Annu. Rev. Med.* 2010; 61:359–373. [PubMed: 20059343] b) Riehemann K, Schneider SW, Luger TA, Godin B, Ferrari M, Fuchs H. *Angew. Chem. Int. Ed.* 2009; 48:872–897. c) Weissleder R, Pittet MJ. *Nature.* 2008; 452:580–589. [PubMed: 18385732] d) Davis ME, Chen Z, Shin DM. *Nat. Rev. Drug Discov.* 2008; 7:771–782. [PubMed: 18758474] e) Peer D, Karp JM, Hong S, Farokhzad OC, Margalit R, Langer R. *Nat. Nanotech.* 2007; 2:751–760.
2. a) Torchilin V. *Eur. J. Pharm. Biopharm.* 2009; 71:431–444. [PubMed: 18977297] b) Lee ES, Gao ZG, Bae YH. *J. Controlled Release.* 2008; 132:164–170.
3. a) Lee ES, Na K, Bae YH. *J. Controlled Release.* 2003; 91:103–113. b) Bae Y, Fukushima S, Harada A, Kataoka K. *Angew. Chem. Int. Ed.* 2003; 42:4640–4643. c) Lynn DM, Amiji MM, Langer R. *Angew. Chem. Int. Ed.* 2001; 40:1707–1710.
4. a) Choi SW, Zhang Y, Xia Y. *Angew. Chem. Int. Ed.* 2010; 49:7904–7908. b) Jeong B, Bae YH, Kim SW. *J. Controlled Release.* 2000; 63:155–163.
5. a) Wang C, Chen Q, Wang Z, Zhang X. *Angew. Chem. Int. Ed.* 2010; 49:8612–8615. b) Olson ES, Jiang T, Aguilera TA, Nguyen QT, Ellies LG, Scadeng M, Tsien RY. *Proc. Natl. Acad. Sci. USA.* 2010; 107:4311–4316. [PubMed: 20160077] c) Bernardos A, Aznar E, Marcos MD, Martínez-Máñez R, Sancenón F, Soto J, Barat JM, Amorós P. *Angew. Chem. Int. Ed.* 2009; 48:5884–5887.
6. a) Li YL, Zhu L, Liu Z, Cheng R, Meng F, Cui JH, Ji SJ, Zhong Z. *Angew. Chem. Int. Ed.* 2009; 48:9914–9918. b) Saito G, Swanson JA, Lee KD. *Adv. Drug Del. Rev.* 2003; 55:199–215.
7. a) Febvay S, Marini DM, Belcher AM, Clapham DE. *Nano Lett.* 2010; 10:2211–2219. [PubMed: 20446663] b) Volodkin DV, Skirtach AG, Mohwald H. *Angew. Chem. Int. Ed.* 2009; 48:1807–1809. c) Skirtach AG, Muñoz Javier A, Kreft O, Köhler K, Piera Alberola A, Möhwald H, Parak WJ, Sukhorukov GB. *Angew. Chem. Int. Ed.* 2006; 45:4612–4617.
8. a) Gatenby RA, Gillies RJ. *Nat Rev Cancer.* 2008; 8:56–61. [PubMed: 18059462] b) Gillies RJ, Raghunand N, Garcia-Martin ML, Gatenby RA. *IEEE Eng. Med. Biol. Mag.* 2004; 23:57–64. [PubMed: 15565800] c) Tannock IF, Rotin D. *Cancer Res.* 1989; 49:4373–4384. [PubMed: 2545340]
9. a) Tian Y, Su F, Weber W, Nandakumar V, Shumway BR, Jin Y, Zhou X, Holl MR, Johnson RH, Meldrum DR. *Biomaterials.* 2010; 31:7411–7422. [PubMed: 20619451] b) Ko JY, Park S, Lee H, Koo H, Kim MS, Choi K, Kwon IC, Jeong SY, Kim K, Lee DS. *Small.* 2010; 6:2539–2544. [PubMed: 20979241] c) Du JZ, Sun TM, Song WJ, Wu J, Wang J. *Angew. Chem. Int. Ed.* 2010; 49:3621–3626. d) Lee ES, Gao ZG, Kim D, Park K, Kwon IC, Bae YH. *J. Controlled Release.* 2008; 129:228–236. e) Sawant RM, Hurley JP, Salmaso S, Kale A, Tolcheva E, Levchenko TS, Torchilin VP. *Bioconjugate Chem.* 2006; 17:943–949. f) Lee ES, Na K, Bae YH. *Nano Lett.* 2005; 5:325–329. [PubMed: 15794620]
10. a) Bae Y, Nishiyama N, Kataoka K. *Bioconjugate Chem.* 2007; 18:1131–1139. b) Potinini A, Lynn DM, Langer R, Amiji MM. *J. Controlled Release.* 2003; 86:223–234. c) Kratz F, Beyer U, Schutte MT. *Crit. Rev. Ther. Drug Carrier Syst.* 1999; 16:245–288. [PubMed: 10706520]
11. a) Zhou ZX, Shen YQ, Tang JB, Fan MH, Van Kirk EA, Murdoch WJ, Radosz M. *Adv. Funct. Mater.* 2009; 19:3580–3589. b) Lee Y, Miyata K, Oba M, Ishii T, Fukushima S, Han M, Koyama H, Nishiyama N, Kataoka K. *Angew. Chem. Int. Ed.* 2008; 47:5163–5166. c) Lee Y, Fukushima S, Bae Y, Hiki S, Ishii T, Kataoka K. *J. Am. Chem. Soc.* 2007; 129:5362–5363. [PubMed: 17408272]
12. a) Nel AE, Madler L, Velegol D, Xia T, Hoek EMV, Somasundaran P, Klaessig F, Castranova V, Thompson M. *Nat Mater.* 2009; 8:543–557. [PubMed: 19525947] b) Maysinger D. *Org. Biomol. Chem.* 2007; 5:2335–2342. [PubMed: 17637950] c) Watson P, Jones AT, Stephens DJ. *Adv. Drug Del. Rev.* 2005; 57:43–61.
13. a) Casey JR, Grinstein S, Orlowski J. *Nat. Rev. Mol. Cell Biol.* 2010; 11:50–61. [PubMed: 19997129] b) Maxfield FR, McGraw TE. *Nat. Rev. Mol. Cell Biol.* 2004; 5:121–132. [PubMed: 15040445]
14. a) Zhou K, Lu Y, Li J, Shen L, Zhang G, Xie Z, Wu C. *Macromolecules.* 2008; 41:8927–8931. b) Riess G. *Prog. Polym. Sci.* 2003; 28:1107–1170. c) Lee ES, Shin HJ, Na K, Bae YH. *J. Controlled Release.* 2003; 90:363–374.

15. a) Kim MS, Hwang SJ, Han JK, Choi EK, Park HJ, Kim JS, Lee DS. *Macromol. Rapid Commun.* 2006; 27:447–451. b) Butun V, Armes SP, Billingham NC. *Polymer.* 2001; 42:5993–6008.
16. a) Tsarevsky NV, Matyjaszewski K. *Chem. Rev.* 2007; 107:2270–2299. [PubMed: 17530906] b) Ma YH, Tang YQ, Billingham NC, Armes SP, Lewis AL, Lloyd AW, Salvage JP. *Macromolecules.* 2003; 36:3475–3484.
17. Albertazzi L, Storti B, Marchetti L, Beltram F. *J. Am. Chem. Soc.* 2010; 132:18158–18167. [PubMed: 21141854]
18. a) Kobayashi H, Ogawa M, Alford R, Choyke PL, Urano Y. *Chem. Rev.* 2010; 110:2620–2640. [PubMed: 20000749] b) Uchiyama S, Iwai K, de Silva AP. *Angew. Chem. Int. Ed.* 2008; 47:4667–4669. c) Lakowicz, JR. *Principles of Fluorescence Spectroscopy*. 3rd. New York City: Springer; 2006. p. 443-475. d) Diaz-Fernandez Y, Foti F, Mangano C, Pallavicini P, Patroni S, Perez-Gramatges A, Rodriguez-Calvo S. *Chem. Eur. J.* 2006; 12:921–930. [PubMed: 16196070]
19. Urano Y, Asanuma D, Hama Y, Koyama Y, Barrett T, Kamiya M, Nagano T, Watanabe T, Hasegawa A, Choyke PL, Kobayashi H. *Nat. Med.* 2009; 15:104–109. [PubMed: 19029979]
20. Atkins P, De Paula J. *Physical Chemistry*, Oxford University Press. 2009
21. Modi S, Swetha MG, Goswami D, Gupta GD, Mayor S, Krishnan Y. *Nat. Nanotech.* 2009; 4:325–330.
22. Gagliardi S, Rees M, Farina C. *Curr. Med. Chem.* 1999; 6:1197–1212. [PubMed: 10519916]

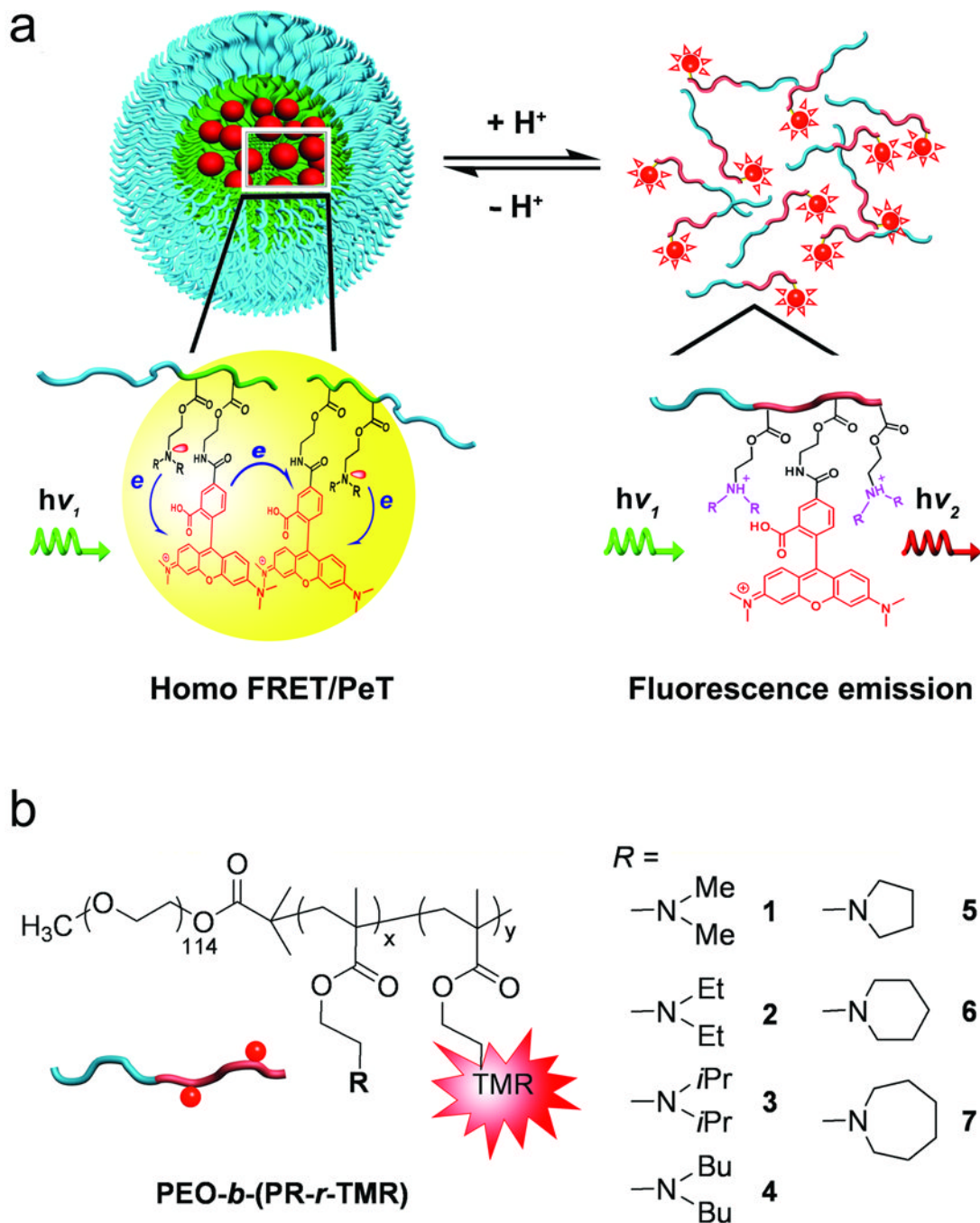


Figure 1.

a) Schematic design of pH-activatable micelle (pHAM) nanoprobe. At $\text{pH} > \text{pKa}$ of ammonium groups (left panel), the neutralized PR segments self-assemble into the micelle cores, leading to quenching of fluorophores due to homoFRET and PeT mechanisms. Upon pH activation ($\text{pH} < \text{pKa}$, right panel), formation of charged ammonium groups results in micelle dissociation into unimers with dramatic increase in fluorescence emission. b) Structures of the PEO-*b*-(PR-*r*-TMR) copolymers in the di-alkyl and cyclic series.

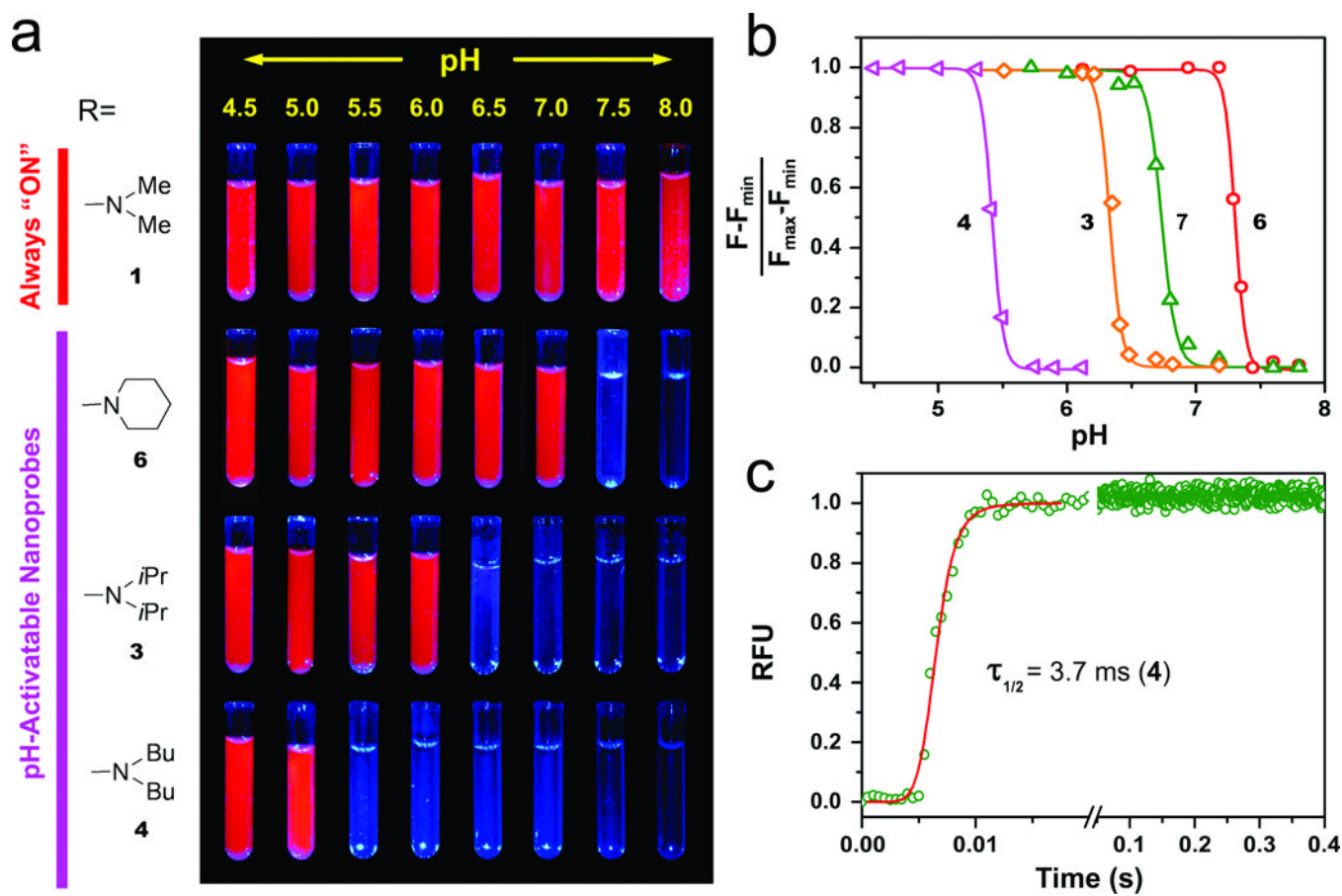


Figure 2.

Illustration of tunable, ultra-pH responsive properties of pHAM nanoprobes. a) Representative fluorescent images of different nanoprobe solutions (**6**, **3**, **4**) at the same polymer concentration (0.1 mg/mL) but different pH values. A narrow pH response is observed for each nanoprobe at different transition pHs. Copolymer **1** serves as an always "ON" control without pH response. A blue light ($\lambda_{\text{ex}} = 440 \sim 480 \text{ nm}$, 450 mW/cm^2) was used to excite the nanoprobes. b) Normalized fluorescence intensity as a function of pH for different pHAM nanoprobes. The pH response ($\Delta\text{pH}_{10-90\%}$) is $< 0.25 \text{ pH unit}$ and $F_{\text{max}}/F_{\text{min}}$ is up to 55-fold (Supplementary Table S2). c) Stopped flow fluorescence measurement of nanoprobe **4** ($\text{pH}_t = 5.4$) after pH activation at 4.9. Fluorescence recovery time ($\tau_{1/2}$) is 3.7 ms. Other pHAM nanoprobes show similarly fast kinetics (Table S2).

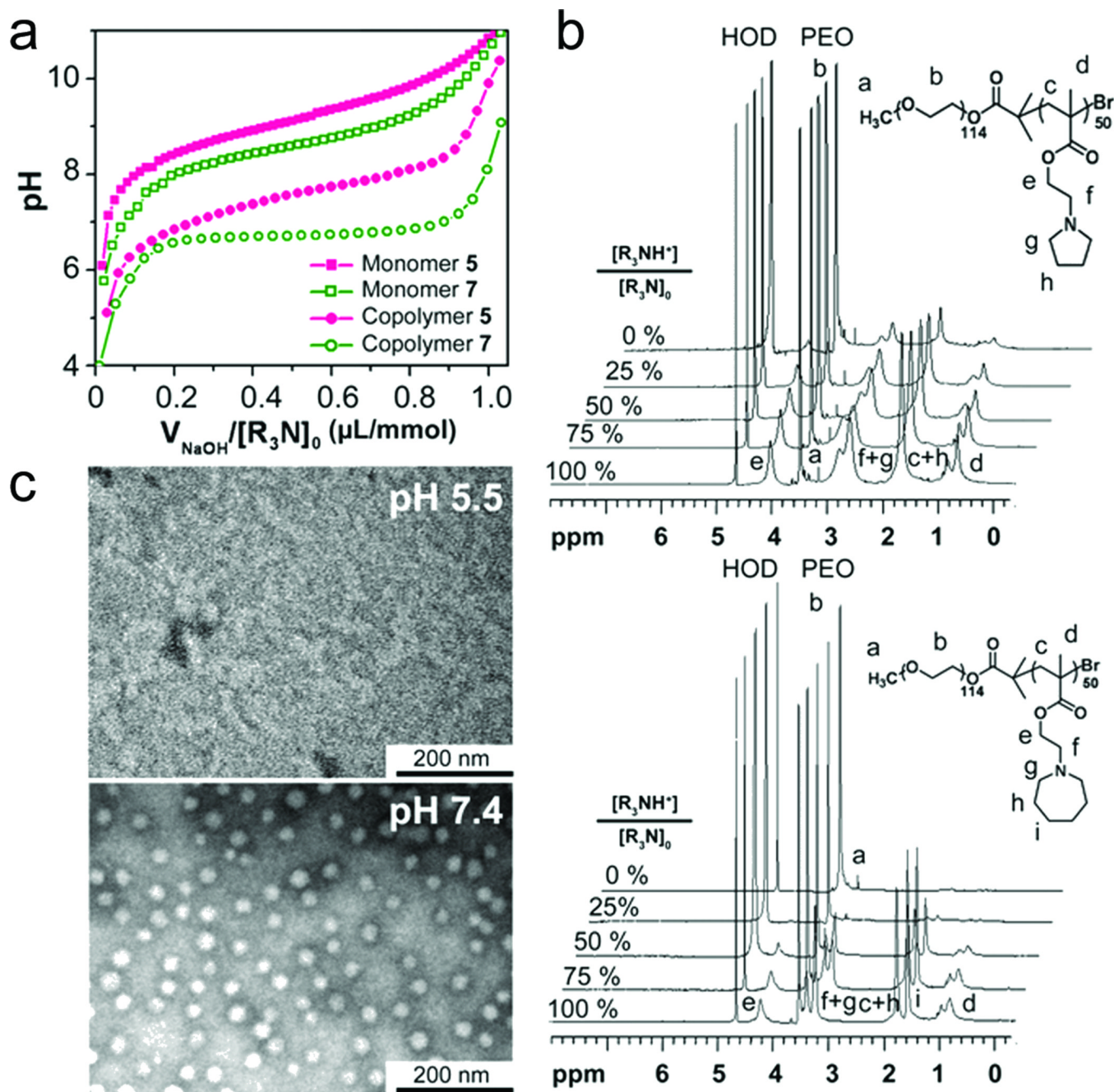
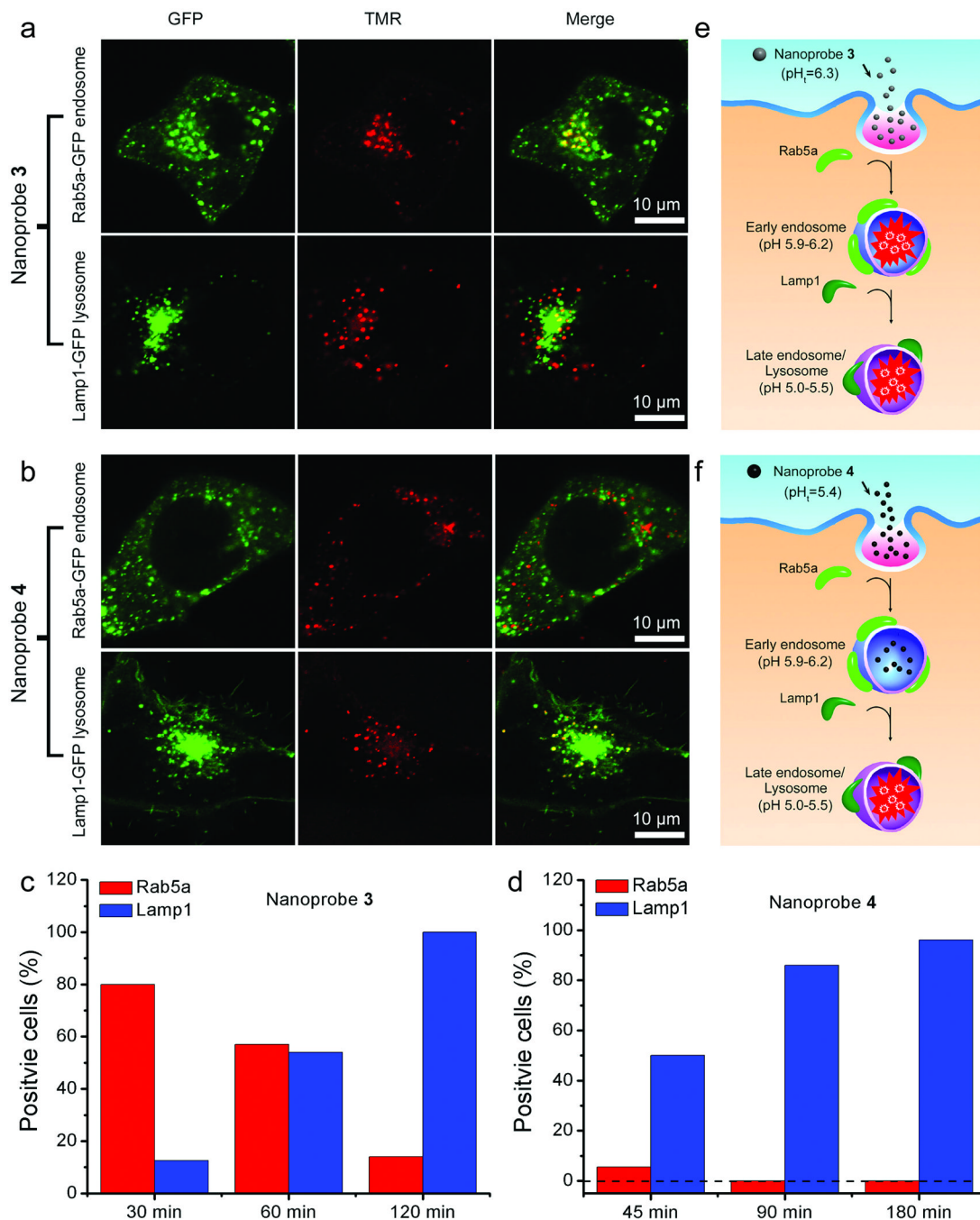


Figure 3. Investigation of the ultra-pH responsive properties of a representative pHAM. a) pH titration curves of copolymers **5** and **7** and their corresponding monomers. The added volumes of NaOH (V_{NaOH}) were normalized to the initial amount of amine residues ($[R_3N]_0$) in mmol. b) ^1H NMR spectra (in D_2O) of **5** and **7** at different ionization states of the copolymers. c) TEM of **7** in pH 5.5 and 7.4 buffers at the polymer concentration of 2 mg/mL.

**Figure 4.**

Investigation of subcellular activation of nanoprobe 3 and 4 in different endocytic organelles in human H2009 cells. a, b) Representative confocal images of activated nanoprobe 3 (a, pH_t = 6.3) and 4 (b, pH_t = 5.4) in cells with GFP-labeled early endosomes (top panel) and late endosomes/lysosomes (bottom panel) at 30 and 45 min, respectively. c, d) Percentage of positive cells (N=30–50 cells) with activated nanoprobe 3 and 4 colocalizing with early endosomes or late endosomes/lysosomes at different incubation times, respectively. e, f) Schematic illustration of the selective activations of nanoprobe 3 in

early endosomes (pH 5.9–6.2) and **4** in late endosomes/lysosomes (pH 5.0–5.5), respectively.

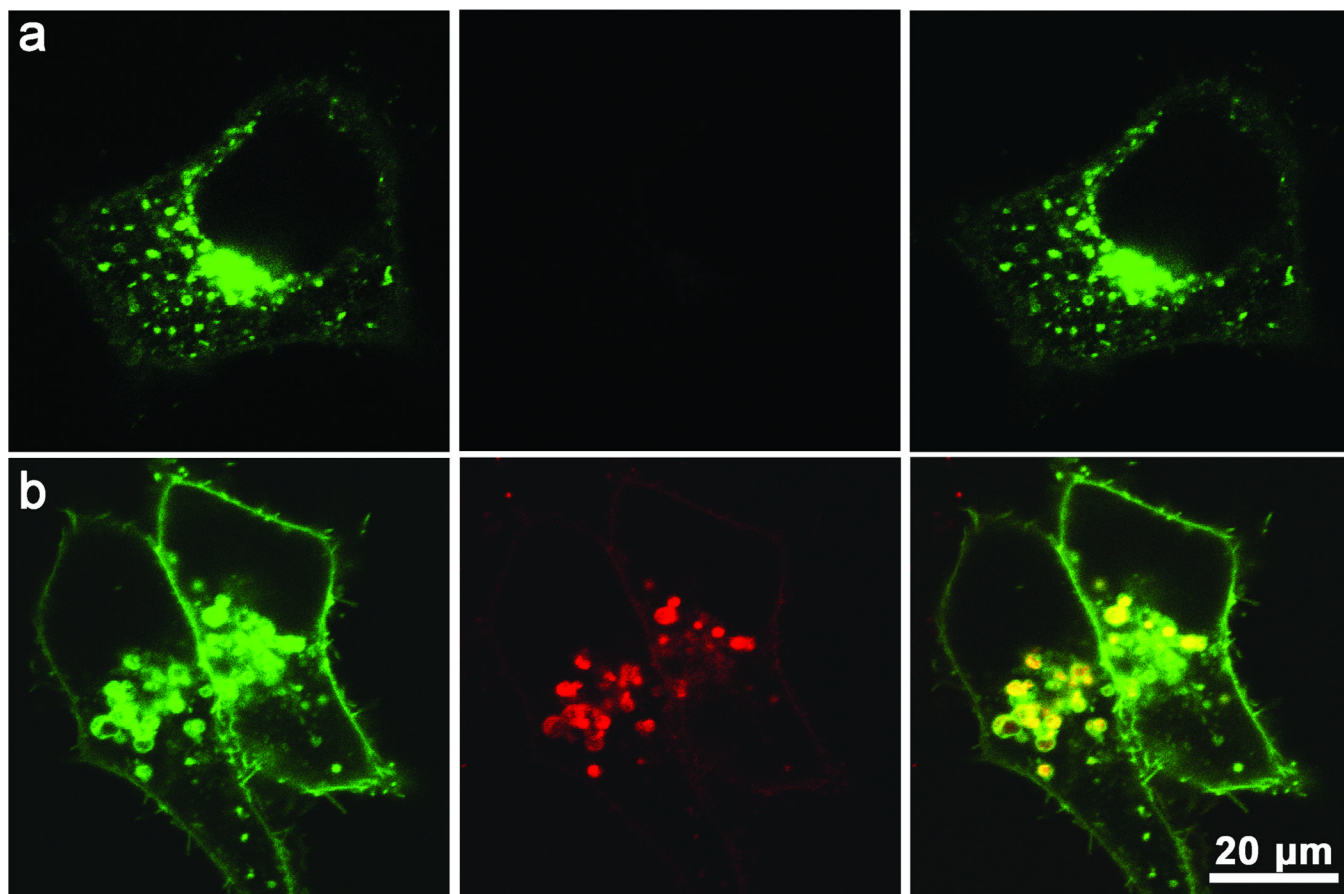


Figure 5. Inhibition of lysosomal acidification by bafilomycin A1 and its effect on intracellular activation of nanoprobe **3** in H2009 cells. a) Confocal images of cells treated with bafilomycin A1 for 1 h followed by nanoprobe **3** incubation for 1 h. Lack of activation of nanoprobe **3** was observed as demonstrated by the absence of TMR fluorescence. b) Confocal images of the same H2009 cells after removal of bafilomycin A1 and nanoprobe **3** and incubation for additional 5 h. Nanoprobe activation was observed as indicated by the red fluorescence inside lysosomes (yellow dots in the overlay images). Scale bar = 20 μm .